

# Reachable Sets for Safe, Real-Time Manipulator Trajectory Design

Patrick Holmes<sup>1</sup>, Shreyas Kousik<sup>1</sup>, Bohao Zhang<sup>1</sup>, Daphna Raz<sup>2</sup>,  
Corina Barbalata<sup>3</sup>, Matthew Johnson-Roberson<sup>2,4</sup>, Ram Vasudevan<sup>1,2</sup>

**Abstract**—For robotic arms to operate in arbitrary environments, especially near people, it is critical to certify the safety of their motion planning algorithms. However, there is often a trade-off between safety and real-time performance; one can either carefully design safe plans, or rapidly generate potentially-unsafe plans. This work presents a receding-horizon, real-time trajectory planner with safety guarantees, called ARMTD (Autonomous Reachability-based Manipulator Trajectory Design). The method first computes (offline) a reachable set of parameterized trajectories for each joint of an arm. Each trajectory includes a fail-safe maneuver (braking to a stop). At runtime, in each receding-horizon planning iteration, ARMTD constructs a reachable set of the entire arm in workspace and intersects it with obstacles to generate sub-differentiable and provably-conservative collision-avoidance constraints on the trajectory parameters. ARMTD then performs trajectory optimization for an arbitrary cost function on the parameters, subject to these constraints. On a 6 degree-of-freedom arm, ARMTD outperforms CHOMP in simulation and completes a variety of real-time planning tasks on hardware, all without collisions.

## I. INTRODUCTION

To maximize utility in arbitrary environments, especially when operating near people, robotic arms should plan collision-free motions in real time. Such performance requires sensing and reacting to the environment as the robot plans and executes motions; in other words, it must perform *receding-horizon planning*, where it iteratively generates a plan while executing a previous plan. This paper addresses **guaranteed-safe receding-horizon trajectory planning for robotic arms**. We call the proposed method **ARMTD** (Autonomous Reachability-based Manipulator Trajectory Design).

### A. Related Work

Motion planning can be broadly split into three paradigms, depending on whether safety is enforced by (1) a path planner, (2) a trajectory planner, or (3) a tracking controller.

The first paradigm is commonly used for robotic arm planning, wherein the path planner is responsible for safety. One generates a collision-free path, then smooths it and parameterizes it by time (i.e., converts it into a trajectory) while obeying joint limits [2], [3]. Such methods often have a tradeoff between

This work is supported by the Ford Motor Company via the Ford-UM Alliance under award N022977, the Office of Naval Research under award number N00014-18-1-2575, and by National Science Foundation Award #1751093.

<sup>1</sup>Mechanical Engineering, University of Michigan, Ann Arbor, MI. <pdholmes, skousik, jimzhang, ramv>@umich.edu

<sup>2</sup>Robotics Institute, University of Michigan, Ann Arbor, MI. daphraz@umich.edu

<sup>3</sup>Mechanical and Industrial Engineering, Louisiana State University, Baton Rouge, LA. cbarbalata@lsu.edu

<sup>4</sup>Naval Architecture and Marine Engineering, University of Michigan, Ann Arbor, MI. mattjr@umich.edu

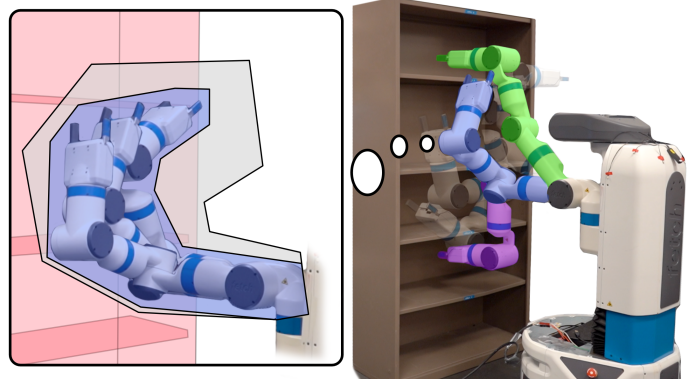


Fig. 1: ARMTD performs safe, real-time receding-horizon planning for a Fetch arm [1] around a cabinet in real time from a start pose (purple, low shelf) to a goal (green, high shelf). Several intermediate poses are shown (transparent). The callout on the left, corresponding to the blue intermediate pose, shows a single planning iteration, with the shelf in light red. In grey is the arm's reachable set given a continuum of parameterized trajectories over a short time horizon. The smaller blue set is the subset of the reachable set corresponding to the particular trajectory that was selected for this planning iteration. Over many such trials in simulation and on hardware, ARMTD never crashed. See the video at <https://youtu.be/ySnux2ow1AA>.

safety and real-time performance because they represent paths with discrete points in configuration space [4], [5]. Ensuring safety requires approximations such as buffering the volume of the arm at each discrete point to account for the discretization, or computing the swept volume along the path assuming, e.g., straight lines between points [6]. If one treats the path as a decision variable in a nonlinear optimization program, the gradient of the distance between the arm's volume and obstacles may "push" each configuration out of collision [7]–[9]. This has the advantage that the output path can be treated directly as a trajectory, if the optimization uses path smoothness as the cost. However, this relies on several approximations to achieve real-time performance: finite differencing to bound joint speeds and accelerations, collision penalties in the cost instead of hard constraints, and finite differencing [7] or linearization [8] for the collision-avoidance penalty gradient. This necessitates finer discretization to faithfully represent the robot's kinematics. To enable real-time performance without gradients, one can compute many paths offline, then collision-check at runtime [10], [11]; but for arbitrary tasks, it can be unclear how many paths are necessary, or how to ensure safety if the arm's volume changes (e.g., by grasping an object). Another approach to real-time performance is to plan iteratively in a receding-horizon either by gradient descent (with the same drawbacks as above) [9] or assuming the underlying path planner is safe [12]. In summary, across this paradigm, one must discretize sufficiently finely, or buffer by a large amount, to achieve safety at the

expense of performance.

In the second paradigm, the path planner generates a (potentially unsafe) path, then the trajectory planner attempts to track the path as closely as possible while maintaining safety. In this paradigm, one computes a *reachable set* (RS) for a family of trajectories instead of computing a swept volume for a path. Methods in this paradigm can achieve both safety and real-time performance in receding-horizon planning by leveraging sums-of-squares programming [13], [14] or zonotope reachability analysis [15]. Unfortunately, the methods in this paradigm suffer from the curse of dimensionality, preventing their use with the high-dimensional models of typical arms.

In the third paradigm, one attempts to ensure safety via the tracking controller, instead of in a path or trajectory. In this paradigm for arms, one builds a supervisory safety controller by pre-specifying planned trajectories [16] or a set of safe states [17]. Another approach in this paradigm is to compute an obstacle safety buffer and associated controller using Hamilton-Jacobi-Bellman reachability analysis [18], [19], but the curse of dimensionality has prevented this from being used for arms.

### B. Proposed Method Summary

Our proposed ARMTD method extends the second planning paradigm to arms by composing RSs online and using them to plan in real time with safety guarantees. The RS representation enables the generation of collision-avoidance, self-intersection, and joint limit constraints with analytic subgradients. Importantly, the RS composition, constraint generation, and gradient evaluation are all parallelizable.

ARMTD begins by specifying a parameterized continuum of kinematic configuration space trajectories, each of which includes a fail-safe maneuver (Section III). Offline, ARMTD computes a parameterized joint reachable set, or JRS, of these trajectories in configuration space. At runtime (in each receding-horizon), it constructs a parameterized RS from the precomputed JRS. ARMTD intersects the RS with obstacles to generate provably-correct collision-avoidance, self-intersection, and joint limit constraints. ARMTD then solves a trajectory optimization program, subject to these constraints, to select a single optimal parameterized trajectory which minimizes an arbitrary cost function. If it cannot find a feasible solution within a prespecified time limit, the arm continues executing the trajectory from its previous planning iteration (which includes a fail-safe maneuver), guaranteeing perpetual safety [12], [14].

### C. Contributions and Paper Organization

Our contributions are threefold. **First**, a method to conservatively construct the RS of a redundant robotic manipulator, with a high-dimensional model, at runtime (Sections III–IV). **Second**, a parallelized method to perform real-time receding-horizon trajectory optimization for an arbitrary cost function, where any feasible trajectory to the problem is provably safe (Section IV) **Third**, a demonstration on various examples in simulation and on hardware, with no collisions (Section V and Supplemental Video). ARMTD also reaches more goals and finds shorter paths than CHOMP [7]. The remaining

sections are Section II (notation and definitions) and Section VI (concluding remarks). A video of ARMTD on hardware is available at <https://youtu.be/ySnux2ow1AA>.

## II. PRELIMINARIES

This section defines notation and representations of an arm and its environment.

### A. Notation

The  $n$ -dimensional real numbers are  $\mathbb{R}^n$ , natural numbers are  $\mathbb{N}$ , the unit circle is  $\mathbb{S}^1$ , and the set of  $3 \times 3$  rotation matrices is  $\text{SO}(3)$ . Let  $U, V$  denote sets. For a point  $p \in U$ ,  $\{p\} \subset U$  denotes the set containing that point. The power set of  $U$  is  $\mathcal{P}(U)$ . The Minkowski sum is  $U \oplus V = \{u + v \mid u \in U, v \in V\}$ . For a matrix  $A \in \mathbb{R}^{n \times n}$  and set  $U \subseteq \mathbb{R}^n$ ,  $AU = \{Au \mid u \in U\}$ . When applied to matrices,  $\prod$  denotes right multiplication as the index increases (e.g.,  $\prod_{i=1}^3 A_i = A_1 A_2 A_3$ ). Greek lowercase letters in angle brackets represent indeterminate variables (e.g.,  $\langle \sigma \rangle$ ). Superscripts on points index elements of a set. Subscripts indicate joint indices or contextual information.

### B. Arm Representation

Consider an arm with  $n_q \in \mathbb{N}$  joints (i.e.,  $n_q$  DOFs) and  $n_q + 1$  links, including the 0<sup>th</sup> link, or *baselink*.

**Assumption 1.** *Each joint is a single-axis revolute joint, attached between a predecessor link and a successor link. The arm is a single kinematic chain from baselink to end effector; link  $i - 1$  is joined to link  $i$  by joint  $i$  for  $i = 1, \dots, n_q$ .*

We make this assumption to simplify exposition. One can treat multi-DOF joints as compound joints between *virtual* links of zero volume. The *configuration space* is denoted  $Q \subseteq \mathbb{S}^{n_q}$ . A *configuration*  $q \in Q$  is a vector  $[q_1, q_2, \dots, q_{n_q}]^T$ . The space of joint velocities is  $\dot{Q} \subset \mathbb{R}^{n_q}$ . There exists a default configuration  $0 \in Q$ . The *workspace*,  $W \subset \mathbb{R}^3$ , is the set of all points in space reachable by any point on the arm in any configuration. Next, we describe the arm as a kinematic chain.

**Definition 2.** *Each link has a local coordinate frame with the origin located at the link's predecessor joint (the baselink's frame is the global frame). The rotation matrix that describes the rotation of link  $i$  relative to link  $i - 1$  (by joint  $i$ ) is  $R_i(q_i) \in \text{SO}(3)$ . The displacement  $l_i \in \mathbb{R}^3$  denotes the position of joint  $i$  on link  $i$  relative to joint  $(i - 1)$  in the frame of link  $i$ . The set  $L_i \subset \mathbb{R}^3$  denotes the volume occupied by the  $i^{\text{th}}$  link, with respect to its predecessor joint, in the frame of link  $i$ .*

**Definition 3.** *Let  $\text{FO}_i : Q \rightarrow \mathcal{P}(W)$  give the forward occupancy of link  $i$ . That is, the  $i^{\text{th}}$  link occupies the volume*

$$\text{FO}_i(q) = \left\{ \sum_{j < i} \left( \prod_{n \leq j} R_n(q_n) l_j \right) \right\} \oplus \left( \prod_{n \leq i} R_n(q_n) L_i \right). \quad (1)$$

Let  $\text{FO} : Q \rightarrow \mathcal{P}(W)$  return the occupancy of the entire arm:

$$\text{FO}(q) = \bigcup_{i=1}^{n_q} \text{FO}_i(q). \quad (2)$$

The first set in (1) gives the position of joint  $(i-1)$  and the second set gives the rotated volume of link  $i$ . As an example, for an arm with  $n_q > 2$ ,  $\text{FO}_i$  can be written:

$$\text{FO}_i(q) = \left\{ R_1(q_1)l_1 + R_1(q_1)R_2(q_2)l_2 + \dots \right. \\ \left. \dots + \prod_{j \leq (i-1)} R_j(q_j)l_{i-1} \right\} \oplus \left( \prod_{j \leq i} R_j(q_j)L_i \right). \quad (3)$$

Typical arms must avoid self-intersection between their links.

**Definition 4.** We specify  $I_{\text{self}} \subset \mathbb{N}^2$  as a set of joint index pairs for which the links can intersect. That is, for  $(i, j) \in I_{\text{self}}$ , there exist  $q \in Q$  such that  $\text{FO}_i(q) \cap \text{FO}_j(q) \neq \emptyset$ .

For example, one may have  $I_{\text{self}} = \{(1,3), (1,4), (2,4)\}$  for an arm with 4 links and three possible self-intersections.

### C. Planning Timing and Environment

Next, we define the timing and environment requirements for ARMTD's receding-horizon trajectory planning.

**Definition 5.** Any trajectory produced by ARMTD is specified over a time interval  $T \subset \mathbb{R}$ . Without loss of generality (WLOG), since time can be shifted to 0 at the beginning of any planned trajectory, we denote  $T = [0, t_f]$ . We further specify that ARMTD must generate a new plan every  $t_{\text{plan}} < t_f$  seconds.

If a new plan cannot be found before  $t_{\text{plan}}$  seconds have elapsed, ARMTD continues executing its previous plan. Since all robots have physical limits, we make the following assumption:

**Assumption 6.** Each joint  $i$  has a minimum and maximum position  $q_{i,\text{lim}}^-$  and  $q_{i,\text{lim}}^+$ , maximum absolute speed  $\dot{q}_{i,\text{lim}}$  and maximum absolute acceleration  $\ddot{q}_{i,\text{lim}}$ . The values  $t_f$  and  $t_{\text{plan}}$  are chosen such that the duration  $(t_f - t_{\text{plan}})$  is large enough for the arm to brake to a stop from its maximum joint speeds using no more than the maximum accelerations.

Assumption 6 ensures that every plan includes a fail-safe maneuver with enough time to bring the arm safely to a stop.

We now specify the arm's environment.

**Definition 7.** An obstacle is a set  $O \subset W$  that describes the volume in space occupied by an object. If the arm's volume is intersecting the obstacle at a configuration  $q \in Q$ , we say the arm is in collision; i.e.,  $\text{FO}(q) \cap O \neq \emptyset$ .

**Assumption 8.** Each obstacle is compact. Obstacles are static with respect to time. At any time, there are at most a finite number of obstacles  $n_{\text{obs}} \in \mathbb{N}$  in the workspace. At any time, the arm has access to a conservative estimate of the size and location of all obstacles in the workspace.

Typical obstacle representations such as octrees [20] or convex polytopes [21] satisfy this assumption. We make this assumption because we are only concerned with planning, not perception. Note, the static assumption is for ease of exposition, and receding-horizon trajectory planners have been extended to dynamic environments [9], [22].

Since we focus primarily on understanding the behavior of configuration space trajectories, we abuse notation and let  $q: T \rightarrow Q$  denote a trajectory plan and let  $q_i$  denote  $i^{\text{th}}$  component of  $q$  which correspond to the trajectory of the  $i^{\text{th}}$  joint. Let  $\mathcal{O} = \{O_1, \dots, O_{n_o}\}$  denote a collection of obstacles. A trajectory is *collision-free* with respect to obstacles if  $\text{FO}(q(t)) \cap O = \emptyset \forall t \in T, \forall O \in \mathcal{O}$ .

### D. Zonotopes, Matrix Zonotopes, and Rotatopes

We now define several types of sets used to represent the arm's RS in Secs. III and IV.

**Definition 9.** A zonotope is a set in  $\mathbb{R}^n$  for which each element is a linear combination of a center  $x \in \mathbb{R}^n$  and generators  $g^1, \dots, g^p \in \mathbb{R}^n, p \in \mathbb{N}$ :

$$Z = \left\{ y \in \mathbb{R}^n \mid y = x + \sum_{i=1}^p \beta^i g^i, -1 \leq \beta^i \leq 1 \right\}. \quad (4)$$

We denote  $Z = (x, g^i, \langle \beta^i \rangle)^p$  as shorthand for a zonotope with center  $x$ , a set of generators  $\{g^i\}_{i=1}^p$ , and a set of indeterminate coefficients  $\{\langle \beta^i \rangle\}_{i=1}^p$  corresponding to each generator. When an indeterminate coefficient  $\langle \beta^i \rangle$  is evaluated, or assigned a particular value, it is written  $\beta^i$ .

**Definition 10.** A matrix zonotope  $M \subset \mathbb{R}^{n \times n}$  is a set of matrices parameterized by a center  $X$  and generators  $G^1, \dots, G^m$ :

$$M = \left\{ A \in \mathbb{R}^{n \times n} \mid A = X + \sum_{j=1}^m G^j \lambda^j, -1 \leq \lambda^j \leq 1 \right\}. \quad (5)$$

We use  $M = (X, G^j, \langle \lambda^j \rangle)^m$  as shorthand for a matrix zonotope with center  $X$ , generators  $\{G^j\}_{j=1}^m$ , and indeterminate coefficients  $\{\langle \lambda^j \rangle\}_{j=1}^m$ .

Note, superscripts are indices, not exponentiation, of matrix zonotope generators.

We use the product of a matrix zonotope with a zonotope to represent the swept volume of rotating links in Sec. IV, hence the following definition:

**Definition 11.** Let  $Z = (x, g^i, \langle \beta^i \rangle)^p$  be a zonotope and  $M = (X, G^j, \langle \lambda^j \rangle)^m$  be a matrix zonotope. Let  $MZ := \{y \in \mathbb{R}^n \mid y = Az, A \in M, z \in Z\} \subset \mathbb{R}^n$ . We call  $MZ$  a rotatope, which can be written:

$$MZ = \left\{ y \in \mathbb{R}^n \mid y = Xx + \sum_i \beta^i Xg^i + \sum_j \lambda^j G^j x + \right. \\ \left. + \sum_{i,j} \beta^i \lambda^j G^j g^i, -1 \leq (\beta, \lambda) \leq 1 \right\}, \quad (6)$$

where  $i = 1, \dots, p$  and  $j = 1, \dots, m$ .

We write  $MZ$  in shorthand as  $MZ = (\hat{x}, \hat{g}^r, \langle \gamma^r \rangle)^s$  where  $\hat{x} = Xx$ ,  $s = (p+1)(m+1) - 1$ , and the rotatope's generator and coefficient sets are

$$\{\hat{g}^r\}_{r=1}^s = \{Xg^1, \dots, Xg^p, G^1x, \dots, G^mx, G^1g^1, \dots, G^mg^p\} \\ \{\langle \gamma^r \rangle\}_{r=1}^s = \{\langle \beta^1 \rangle, \dots, \langle \beta^p \rangle, \langle \lambda^1 \rangle, \dots, \langle \lambda^m \rangle, \langle \beta^1 \lambda^1 \rangle, \dots, \langle \beta^p \lambda^m \rangle\}.$$

Rotatopes are a special class of polynomial zonotopes [23]. Each  $\langle \gamma^r \rangle$  for  $r > p + m$  is a product of indeterminate coefficients from  $M$  and  $Z$ . For a pair of indeterminate coefficients  $\langle \gamma^1 \rangle$  and  $\langle \gamma^2 \rangle$ , the notation  $\langle \gamma^1 \gamma^2 \rangle$  indicates the product  $\langle \gamma^1 \rangle \langle \gamma^2 \rangle$ . We call  $\langle \gamma^1 \rangle$  and  $\langle \gamma^2 \rangle$  the *factors* of  $\langle \gamma^1 \gamma^2 \rangle$ .

Two useful properties follow directly from the zonotope and rotatope definitions:

**Lemma 12.** *The product of a matrix zonotope with a rotatope is a rotatope.*

**Lemma 13.** (Minkowski sums) *Let  $X = (x, g_X^i, \langle \zeta^i \rangle)^n$  and  $Y = (y, g_Y^j, \langle \psi^j \rangle)^m$ . Then  $X \oplus Y = (x + y, \{g_X^i, g_Y^j\}_{i=1, j=1}^{i=n, j=m}, \{\langle \zeta^i \rangle, \langle \psi^j \rangle\}_{i=1, j=1}^{i=n, j=m})$ , which is a zonotope centered at  $x + y$  with all the generators and indeterminates of both  $X$  and  $Y$ . Similarly, for two rotatopes,  $V = (v, g_V^i, \langle \mu^i \rangle)^n$  and  $W = (w, g_W^j, \langle \omega^j \rangle)^m$ ,*

$$V \oplus W = (v + w, \{g_V^i, g_W^j\}_{i=1, j=1}^{i=n, j=m}, \{\langle \mu^i \rangle, \langle \omega^j \rangle\}_{i=1, j=1}^{i=n, j=m}). \quad (7)$$

One can reindex the generators and indeterminates if necessary.

We often overapproximate rotatopes with zonotopes:

**Lemma 14.** *Any rotatope  $MZ$  as in (6) can be overapproximated by a zonotope.*

*Proof:* Consider the components of the indeterminate coefficients of  $MZ = (x, g^r, \langle \gamma^r \rangle)^s$  that can be written as  $\langle \beta^i \lambda^j \rangle$ . When evaluated,  $\beta^i \lambda^j \in [-1, 1]$ . Consider a zonotope  $\hat{Z} = (x, g^r, \langle \sigma^r \rangle)^s$  with the same center and generators as  $MZ$ , but where each product  $\langle \beta^i \lambda^j \rangle$  is replaced with a single new symbolic coefficient  $\langle \sigma^r \rangle$ . If  $z \in MZ$ ,  $\exists \sigma^r \in [-1, 1]$  such that  $z \in \hat{Z}$ . ■

In Sec. IV, we use the intersection of zonotopes to generate collision-avoidance constraints:

**Lemma 15.** [24, Lem. 5.1] *Given two zonotopes  $X = (x, g^i, \langle \beta^i \rangle)^n$  and  $Y = (y, g^j, \langle \beta^j \rangle)^m$ ,  $X \cap Y \neq \emptyset$  iff  $y$  is in the zonotope  $X_{\text{buf}} = (x, g^i, \langle \beta^i \rangle)^n \oplus (0, g^j, \langle \beta^j \rangle)^m$ .*

The subscript indicates  $X$  is *buffered* by the generators of  $Y$ .

**Remark 16.** *Since zonotopes are convex polytopes [24], one can implement Lem. 15 by computing a half-space representation  $(A_{\text{buf}}, b_{\text{buf}})$  of  $X_{\text{buf}}$  for which  $A_{\text{buf}}z - b_{\text{buf}} \leq 0 \iff z \in X_{\text{buf}}$  [25, Theorem 2.1], where the inequality is taken elementwise. Therefore,  $X \cap Y = \emptyset \iff \max(A_{\text{buf}}y - b_{\text{buf}}) > 0$ .*

### E. Slicing

ARMTD uses zonotopes and rotatopes to represent RSs of parameterized trajectories of an arm. In Sec. IV, our trajectory optimization implementation requires fixing the value of the trajectory parameters to produce a subset of the RS corresponding to any particular trajectory. We call this operation *slicing*, because it takes in a zono/rotatope, evaluates some (or all) of its coefficients, and returns a zono/rotatope that is a subset of the original with potentially fewer (or no) generators. To define slicing, we require the following operations:

**Definition 17.** *Let  $n \in \mathbb{N}$ . We denote the removal of the  $i^{\text{th}}$  factor of the indeterminate  $\langle \gamma^1 \gamma^2 \dots \gamma^n \rangle$  as:*

$$\langle \gamma^1 \gamma^2 \dots \gamma^n \rangle \setminus \langle \gamma^i \rangle = \langle \gamma^1 \gamma^2 \dots \gamma^{i-1} \gamma^{i+1} \dots \gamma^n \rangle. \quad (8)$$

---

**Algorithm 1**  $Z_{\text{sliced}} = \text{slice}(Z, \{\langle \sigma^j \rangle\}_{j=1}^n, \{\sigma^j\}_{j=1}^n)$

---

```

1: // Let  $Z = (x, g^i, \beta^i)^p$  denote the input zonotope or rotatope
2:  $Z_{\text{sliced}} \leftarrow (x, g^i, \beta^i)^p$  // allocate output
3: for  $i = 1, \dots, p$  // iterate over generator/indeterminate pairs
4:   for  $j = 1, \dots, n$  // iterate over input values
5:     if  $\langle \sigma^j \rangle \in \langle \beta^i \rangle$ 
6:        $g^i \leftarrow \sigma^j g^i$  // multiply generator by value
7:        $\langle \beta^i \rangle \leftarrow \langle \beta^i \rangle \setminus \langle \sigma^j \rangle$  // remove evaluated indeterminate
8:     end if
9:   end for
10:  if  $\langle \beta^i \rangle = \emptyset$  // if fully-sliced
11:     $x \leftarrow x + g^i$  // shift center
12:     $g^i \leftarrow \emptyset$  // generator is no longer needed
13:  end if
14: end for

```

---

We define  $\langle \gamma^1 \gamma^2 \dots \gamma^n \rangle \setminus \langle \gamma^1 \gamma^2 \dots \gamma^n \rangle = \emptyset$ . We define  $\langle \sigma \rangle \in \langle \gamma^1 \gamma^2 \dots \gamma^n \rangle$  to mean that  $\langle \sigma \rangle$  is a factor of  $\langle \gamma^1 \gamma^2 \dots \gamma^n \rangle$ .

**Definition 18.** *Consider a zono/rotatope  $Z = (x, g^i, \langle \beta^i \rangle)^p$  and a collection of indeterminate coefficients  $\{\langle \sigma^j \rangle\}_{j=1}^n$  for  $n \in \mathbb{N}$ . A generator  $g^i$  is  $\langle \sigma^j \rangle$ -sliceable if  $\langle \sigma^j \rangle \in \langle \beta^i \rangle$ . We say  $g^i$  is fully-sliced if all of its indeterminate coefficients in  $\langle \beta^i \rangle$  are evaluated.*

We define the `slice` function in Alg. 1 using indeterminate evaluation and removal. This function takes in a zono/rotatope  $Z = (x, g^i, \langle \beta^i \rangle)^p$ , a set of indeterminate coefficient  $\{\langle \sigma^j \rangle\}_{j=1}^n$ , and a set of values for the indeterminate coefficients  $\{\sigma^j\}_{j=1}^n$ , and outputs a sliced zono/rotatope. For each generator in  $Z$ , if  $\langle \sigma^j \rangle$  is a factor of that generator's coefficients, then the generator is multiplied by the value  $\sigma^j$ . If a generator becomes fully-sliced (and therefore has no more indeterminate coefficients), it is added to the center of the output zono/rotatope, and removed from the set of generators. For zonotopes, each generator becomes fully-sliced if its coefficient is evaluated because each coefficient has only one factor. If a rotatope is sliced until each generator has only one coefficient factor, the rotatope becomes a zonotope.

## III. OFFLINE REACHABILITY ANALYSIS

ARMTD uses short parameterized trajectories of the joint angles for online trajectory planning. We begin with a theoretical overview, defining the properties that the parameterized trajectories must satisfy, as well as the Joint Reachable Set (JRS) representing a family of parameterized joint trajectories. We then describe the specific implementation used in this paper, and describe how to represent the JRS with zonotope reachability analysis.

### A. Theory

#### 1) Trajectory Parameterization:

**Definition 19.** *Let  $K \subset \mathbb{R}^{n_k}$ ,  $n_k \in \mathbb{N}$ , denote a compact space of trajectory parameters. Each  $k \in K$  parameterizes a configuration trajectory  $q : T \rightarrow \mathcal{Q}$ . The configuration parameterized by  $k \in K$  at time  $t \in T$  is  $q(t; k)$ . We require  $q(\cdot; k)$  to satisfy*

three properties for all  $k \in K$ . First,  $q(\cdot; k)$  is at least once-differentiable with respect to time. Second,  $q(0; k) = 0$ . Third,  $\dot{q}(t_f; k) = 0$ .

These parameterized trajectories are functions only of time for each parameter  $k \in K$ . In addition, they specify the arm's kinematics, with no notion of dynamics. This is a common approach in motion planning [7]–[11], because existing controllers can track kinematic trajectories closely (e.g., within 0.01 rad for revolute joints [26], [27]) in the absence of disturbances such as collisions. We find these kinematic trajectories sufficient to ensure no collisions in real-world hardware demonstrations (Sec. V). Also, note that methods exist for quantifying tracking error using zonotopes [27] and accounting for it at runtime [15]. The second property in the definition of the trajectory parameter leverages the fact that trajectories can evolve from  $q(0; k) = 0$  without loss of generality, because  $\dot{q}(\cdot; k)$  does not depend on  $q$ . That is, we can always transform the coordinate system of each link at the beginning of each planning iteration to ensure that the initial angle is 0. The third property guarantees that each parameterized trajectory includes a fail-safe braking maneuver (satisfying Assum. 6). We account for joint limits in Sec. IV.

2) *Joint Reachable Sets*: Because each  $q_i$  represents a rotation, we examine the trajectories of  $\cos(q_i)$  and  $\sin(q_i)$ . By Def. 19,  $q(\cdot; k)$  is at least once differentiable. We can write a differential equation of the sine and cosine as a function of the joint trajectory, where  $k$  is a constant:

$$\frac{d}{dt} \begin{bmatrix} \cos(q_i(t)) \\ \sin(q_i(t)) \\ k \end{bmatrix} = \begin{bmatrix} -\sin(q_i(t))\dot{q}_i(t; k) \\ \cos(q_i(t))\dot{q}_i(t; k) \\ 0 \end{bmatrix}. \quad (9)$$

We then define the parameterized JRS of the  $i^{\text{th}}$  joint:

$$\mathcal{J}_i = \left\{ (c, s, k) \in \mathbb{R}^2 \times K \mid \exists t \in T \text{ s.t. } q_i \text{ as in Def. 19,} \right. \\ c = \cos(q_i(t; k)), \quad s = \sin(q_i(t; k)), \quad (10) \\ \left. \text{and } \frac{d}{dt}(\cos(q_i(t)), \sin(q_i(t)), k) \text{ as in (9)} \right\}.$$

We account for different initial joint angles in Sec. IV (see (15)), by leveraging the properties in Def. 19. We use each JRS to overapproximate the forward occupancy map (1) in Sec. IV.

## B. Implementation

We now present a particular trajectory parameterization, and a representation of the corresponding JRS as in (10).

1) *Trajectory Parameterization*: While any parameterization satisfying Def. 19 could be used, we choose a parameterization that is simple, yet sufficient to enable an arm to plan safely in arbitrary scenarios (see Sec. V). We define a *velocity parameter*  $k^v \in \mathbb{R}^{n_q}$  that specifies the initial velocity  $\dot{q}$ , and an *acceleration parameter*  $k^a \in \mathbb{R}^{n_q}$  that specifies a constant acceleration over the time horizon  $[0, t_{\text{plan}})$ . We denote  $k = [k^v, k^a]^\top \in K \subset \mathbb{R}^{n_k}$ , where  $n_k = 2n_q$ . Let  $K_i$  denote the parameters for joint  $i$ . We write  $k^v = [k_1^v, \dots, k_{n_q}^v]^\top$  and similarly for  $k^a$ . The trajectories

are given by

$$\dot{q}(t; k) = \begin{cases} k^v + k^a t, & t \in [0, t_{\text{plan}}) \\ \frac{k^v + k^a t_{\text{plan}}}{t_f - t_{\text{plan}}}(t_f - t), & t \in [t_{\text{plan}}, t_f], \end{cases} \quad (11)$$

with  $q_i(0; k) = 0$  for all  $k$  to satisfy Def. 19. These trajectories brake to a stop over  $[t_{\text{plan}}, t_f]$  with constant acceleration. We require that  $K$  is compact to perform reachability analysis. In particular, for each joint  $i$ , we specify  $K_i = K_i^v \times K_i^a$ , where

$$K_i^v = [\bar{k}_i^v - \Delta k_i^v, \bar{k}_i^v + \Delta k_i^v], \quad K_i^a = [\bar{k}_i^a - \Delta k_i^a, \bar{k}_i^a + \Delta k_i^a], \quad (12)$$

with  $\bar{k}_i^v, \bar{k}_i^a, \Delta k_i^v, \Delta k_i^a \in \mathbb{R}$  and  $\Delta k_i^v, \Delta k_i^a \geq 0$ .

2) *Reachability Analysis*: We represent (10) using zonotopes. To do this, we first select  $\Delta t \in \mathbb{R}$  such that  $\frac{t_f}{\Delta t} \in \mathbb{N}$  and partition  $T$  into  $\frac{t_f}{\Delta t}$  closed intervals each of length  $\Delta t$ , indexed by  $\mathbb{N}_T = \{0, 1, \dots, \frac{t_f}{\Delta t} - 1\}$ . We represent  $\mathcal{J}_i$  with one zonotope per time interval, which is returned by the map  $J_i: \mathbb{N}_T \rightarrow \mathcal{P}(\mathbb{R}^2 \times K)$ . For example, the zonotope  $J_i(n)$  corresponds to the time interval  $[n\Delta t, (n+1)\Delta t]$ . To understand the codomain of  $J_i$ , note that the zonotopes *overapproximate* the values attained by  $\sin(q_i(\cdot))$  and  $\cos(q_i(\cdot))$  during a trajectory; that is, the zonotopes contain points not on the unit circle (see Fig. 2.)

**Remark 20.** We abuse notation and let  $t$  index the subinterval of  $T$  that contains it, so that  $J_i(t) = J_i(\lfloor t/\Delta t \rfloor)$  where  $\lfloor \cdot \rfloor$  rounds a real number down to the nearest integer. We use similar notation for the center, generators, and indeterminates.

We make an initial condition set  $J_i(0) \subset \mathbb{R}^2 \times K$  as a zonotope:

$$J_i(0) = \left( \bar{x}_i, \left\{ \bar{g}_i^v, \bar{g}_i^a \right\}, \left\{ \langle \bar{k}_i^v \rangle, \langle \bar{k}_i^a \rangle \right\} \right), \text{ with} \\ \bar{x}_i = [1, 0, \bar{k}_i^v, \bar{k}_i^a]^\top, \quad (13) \\ \bar{g}_i^v = [0, 0, \Delta k_i^v, 0]^\top, \text{ and } \bar{g}_i^a = [0, 0, 0, \Delta k_i^a]^\top.$$

The indeterminates  $\langle \bar{k}_i^v \rangle$  and  $\langle \bar{k}_i^a \rangle$  correspond to  $\bar{g}_i^v$  and  $\bar{g}_i^a$  respectively.  $J_i(0)$  contains  $K_i^v$  and  $K_i^a$  in the  $k_i^v$  and  $k_i^a$  dimensions.

We use an open-source toolbox [23] with the time partition, dynamics (9) and (11), and initial set zonotope  $J_i(0)$  to overapproximate (10). Importantly, as a result of [25, Thm. 3.3 and Prop. 3.7] one can prove that the zonotope representation is an overapproximation:

**Lemma 21.**

$$\mathcal{J}_i \subseteq \bigcup_{t \in T} J_i(t), \quad (14)$$

i.e.,  $\bigcup_{t \in T} J_i(t)$  in (14) contains all  $(c, s, k) \in \mathcal{J}_i$ .

We now describe a useful property of this zonotope JRS:

**Lemma 22.** *There exist  $J_i: \mathbb{N}_T \rightarrow \mathcal{P}(\mathbb{R}^2 \times K)$  that overapproximate  $\mathcal{J}_i$  as in (14) such that, for each  $t \in T$ ,  $J_i(t)$  has only one generator with a nonzero element, equal to  $\Delta k_i^v$ , in the dimension corresponding to  $k_i^v$ , and only one (distinct) generator with a nonzero element,  $\Delta k_i^a$ , for  $k_i^a$ .*

*Proof:* Given  $J_i(0)$ , the subsequent zonotope  $J_i(\Delta t)$  is computed as  $J_i(\Delta t) = e^{F\Delta t} J_i(0) + E$ , where  $F$  is found by

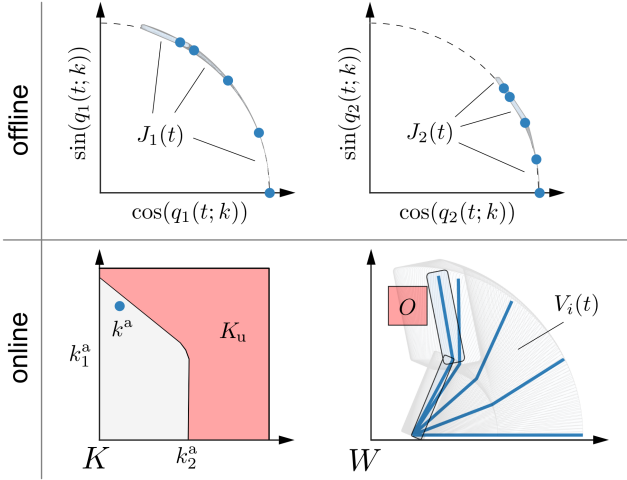


Fig. 2: An overview of the proposed method for a 2-D, 2-link arm. Offline, ARMTD computes the JRS, shown as the collection of small grey sets  $J_i(t)$  overlaid on the unit circle (dashed) in the sine and cosine spaces of two joint angles. Note that these JRS are in fact conservative approximations. Online, the obstacle  $O$  (light red) is mapped to the unsafe set of trajectory parameters  $K_u \subset K$  on the left, by intersection with arm’s reachable set  $V_i(t)$  (large light grey set in  $W$ ). The parameter  $k^a$  represents a trajectory, shown at five time steps (blue arms in  $W$ , and blue dots in joint angle space). The subset of the reachable set corresponding to  $k^a$  is shown for the last time step (light blue boxes with black border), critically not intersecting the obstacle.

linearizing the dynamics (9) at  $t = 0$  and  $E$  is a set that overapproximates the linearization error and the states reached over the interval  $[0, \Delta t]$  [25, Section 3.4.1]. This linearized forward-integration and error-bounding procedure is applied to  $J_i(\Delta t)$  to produce  $J_i(2\Delta t)$ , and so on, to compute all  $J_i(t)$  in (14). Since  $\dot{k} = 0$ , we have that  $e^{F\Delta} \tilde{g}_i^v$  equals  $\tilde{g}_i^v$  in the  $k$  dimensions (and therefore each  $g_i^v(t)$  does as well, and similarly for  $g_i^a(t)$ ). Since the zero dynamics have no linearization error, one can define  $E$  to have zero volume in the  $k$  dimensions [25, Proposition 3.7], meaning no generator of any  $J_i(t)$  has a nonzero element in the  $k$  dimensions except for  $g_i^v(t)$  and  $g_i^a(t)$ . ■

Note, the zonotopes created by the open-source toolbox [23] satisfy the requirements of Lem. 22.

**Remark 23.** For all  $t$  except 0,  $g_i^v(t)$  and  $g_i^a(t)$  may have nonzero elements in the cosine and sine dimensions, due to the nonzero dynamics and linearization error in those dimensions.

We call  $g_i^v(t)$  and  $g_i^a(t)$   $k$ -sliceable. For each  $J_i(t)$ , we denote the center  $x_i(t)$ , the generators  $\{g_i^v(t), g_i^a(t), g_i^j(t)\}$ , and the indeterminates  $\{\langle \kappa_i^v(t) \rangle, \langle \kappa_i^a(t) \rangle, \langle \beta_i^j(t) \rangle\}$  for  $j = 1, \dots, p(t) \in \mathbb{N}$ . We write  $p(t)$  since the number of generators is not necessarily the same for each  $J_i(t)$  [23]. Next, we use the JRS for online planning.

#### IV. ONLINE PLANNING

This section presents ARMTD’s online planning algorithm for a single receding-horizon iteration in three steps as depicted in Fig. 2. We begin with a theoretical overview, then discuss our implementation. First, in each planning iteration, we construct the parameterized RS of the full arm from the parameterized

JRS of each joint; in implementation, we use each JRS to compute an overapproximation of the forward occupancy map (2). Second, we identify the set of unsafe trajectories that could cause collisions (or self-intersections) by intersecting the arm’s parameterized RS with obstacles (and itself). Third, we optimize over the set of safe trajectories to minimize an arbitrary cost function. If no solution is found, we execute the previous plan’s fail-safe maneuver.

#### A. Theory

1) *Reachable Set Construction:* As mentioned in Sec. I, computing the workspace RS of an arm *offline* is challenging because the initial condition space is high-dimensional. Our solution is to use the initial conditions  $(\tilde{q}, \dot{\tilde{q}}) \in Q \times \dot{Q}$  of the current planning iteration to compose the RS of the arm *online* from the low-dimensional JRSs (computed offline).

First, we introduce a link RS  $\mathcal{L}_i$ ; for the  $i^{\text{th}}$  link, it is formed from all JRSs  $\mathcal{J}_j$  with  $j \leq i$ , since the position and orientation of the  $i^{\text{th}}$  link depends on all predecessor joints:

$$\mathcal{L}_i = \left\{ (Y, k) \in \mathcal{P}(W) \times K \mid \exists t \in T \text{ s.t.} \right. \\ \left. \begin{aligned} \dot{q}_i(0; k) = \dot{\tilde{q}}_i, \quad Y = \text{FO}_i(q(t; k) + \tilde{q}), \\ \text{and } (\cos(q_j(t; k)), \sin(q_j(t; k)), k) \in \mathcal{J}_j \quad \forall j \leq i \end{aligned} \right\} \quad (15)$$

with  $\text{FO}_i$  as in Def. 3. Each  $\mathcal{L}_i$  is formed using only trajectories which start at the given initial conditions  $(\tilde{q}, \dot{\tilde{q}})$ . The RS of the entire arm,  $\mathcal{L} \subset W \times K$ , is then given by  $\mathcal{L} = \bigcup_i \mathcal{L}_i$ .

2) *Constraint Generation:* Second, ARMTD uses  $\mathcal{L}$  to find all unsafe trajectory parameters  $k \in K_u \subseteq K$  that could cause collisions with obstacles and self-intersections. ARMTD generates constraints to avoid  $K_u$ , which includes additional constraints enforcing joint angle/velocity limits.

Let  $I_{\text{self}} \subset \mathbb{N}^2$  be a set of link index pairs that define self-intersections (Def. 4). Let  $\mathcal{O}$  be a collection of obstacles as in Def. 7, and let  $q_{i, \text{lim}}^-, q_{i, \text{lim}}^+$  and  $\dot{q}_{i, \text{lim}}$  be defined as in Assum. 6. At each planning iteration, the subset of unsafe trajectory parameters is:

$$K_u = K_{\text{obs}} \cup K_{\text{self}} \cup K_{\text{lim}}, \quad \text{where} \quad (16)$$

$$K_{\text{obs}} = \{k \mid Y \cap O \neq \emptyset, (Y, k) \in \mathcal{L}, O \in \mathcal{O}\} \quad (17)$$

$$K_{\text{self}} = \{k \mid Y_i \cap Y_j \neq \emptyset, (i, j) \in I_{\text{self}}, \\ (Y_i, k) \in \mathcal{L}_i, \text{ and } (Y_j, k) \in \mathcal{L}_j\} \quad (18)$$

$$K_{\text{lim}} = \{k \mid \exists t \in T \text{ s.t. } q(t; k) < q_{i, \text{lim}}^- \text{ or } q(t; k) > q_{i, \text{lim}}^+ \\ \text{or } |\dot{q}(t; k)| > \dot{q}_{i, \text{lim}}\}. \quad (19)$$

3) *Trajectory Optimization:* Third, ARMTD performs trajectory optimization over  $K \setminus K_u$  for an arbitrary user-specified cost function  $f : K \rightarrow \mathbb{R}$  (which encodes information such as completing a task). ARMTD attempts to solve the following program within the duration  $t_{\text{plan}}$ :

$$k_{\text{opt}} = \operatorname{argmin}_k \{f(k) \mid k \notin K_u\}. \quad (20)$$

If no solution is found in time, ARMTD executes the fail-safe maneuver found during the previous planning iteration.

## B. Implementation

Before implementing the theory above, we briefly note that, in our receding-horizon framework, ARMTD is planning while the robot is executing its previous plan. Therefore, ARMTD must estimate its future initial conditions  $(\tilde{q}, \dot{\tilde{q}})$  as a result of its previous plan by integrating (11) forward for  $t_{\text{plan}}$  seconds.

1) *Reachable Set Construction*: Because we use the RS of the arm,  $\mathcal{L}$ , to find trajectories that can cause collisions, it is important that we overapproximate  $\mathcal{L}$  to guarantee safety. We have shown that we conservatively overapproximate each JRS  $\mathcal{J}_i$  in Lem. 21, and leverage this property to generate a conservative overapproximation of  $\mathcal{L}$  represented by a set of rotatopes with Alg. 2.

First, we slice the JRS zonotopes (see Alg. 1) to ensure we only consider trajectories that begin from the correct initial velocity  $\dot{\tilde{q}}$ . Note that  $\dot{\tilde{q}} \in K_v$  is enforced by the constraints generated later in this section. For each joint  $i$ , recall that each  $J_i(t)$  has generator  $g_i^v(t)$ , with indeterminate  $\langle \kappa_i^v(t) \rangle$  and nonzero element  $\Delta k_i^v$  corresponding to the  $k_i^v$  dimension. Also,  $x_i(t)$  has the value of  $\overline{k_i^v}$  in that same dimension. We slice each  $J_i(t)$ :

$$S_i(t) = \text{slice} \left( J_i(t), \langle \kappa_i^v(t) \rangle, \frac{\dot{\tilde{q}} - \overline{k_i^v}}{\Delta k_i^v} \right) \quad (21)$$

$$= \left( x_i^v(t), \{g_i^a(t), g_i^j(t)\}, \{\langle \kappa_i^a(t) \rangle, \langle \beta_i^j(t) \rangle\} \right)^{p(t)} \quad (22)$$

where  $x_i^v(t)$  is the new (shifted) center and  $p(t) \in \mathbb{N}$  is the new number of generators, other than  $g_i^a(t)$ , left after slicing.

$S_i(t)$  now contains a set of  $\cos(q_i(t; k))$  and  $\sin(q_i(t; k))$  reachable for a single value of  $k_i^v$ , but for a range of  $k_i^a$ . Denote  $S_i(t)$  as in (22) with  $x_i^v(t) = [c_i^v, s_i^v, \dot{\tilde{q}}_i, \overline{k_i^v}]^T$ ,  $g_i^a(t) = [c_i^a, s_i^a, 0, \Delta k_i^a]^T$  and  $g_i^j(t) = [c_i^j, s_i^j, 0, 0]^T$  for each  $j = 1, \dots, p(t)$ . From Rem. 23, the components  $c_i^a$  and  $s_i^a$  are generally non-zero, and  $\Delta k_i^a$  is constant from Lem. 22.

The forward occupancy map (2) relies on the multiplication of rotation matrices formed from the cosine and sine of each joint; by multiplying overapproximations of these rotation matrices, we overapproximate the forward occupancy map for the set of configurations encoded in each  $S_i(t)$ . We use each sliced zonotope  $S_i(t)$  to produce a matrix zonotope  $M_i(t)$  that overapproximates a set of rotation matrices corresponding to joint  $i$  at time  $t$ . We do so by reshaping the center and generators of  $S_i(t)$  (and keeping its indeterminates), then rotating the resulting matrix zonotope by the initial joint angle  $\tilde{q}$ ; we call this the `makeMatZono` function in Alg. 3. For example, suppose joint  $i$  rotates about its predecessor link's 3-axis (in Euler angle notation as in [6, (3.39)]):

$$M_i(t) = R_i(\tilde{q}_i) \left( X_i^v(t), \{G_i^a(t), G_i^j(t)\}, \{\langle \kappa_i^a(t) \rangle, \langle \beta_i^j(t) \rangle\} \right)^{p(t)}, \quad (23)$$

$$X_i^v(t) = \begin{bmatrix} c_i^v & -s_i^v & 0 \\ s_i^v & c_i^v & 0 \\ 0 & 0 & 1 \end{bmatrix}, \quad G_i^a(t) = \begin{bmatrix} c_i^a & -s_i^a & 0 \\ s_i^a & c_i^a & 0 \\ 0 & 0 & 0 \end{bmatrix}, \quad (24)$$

$$G_i^j(t) = \begin{bmatrix} c_i^j & -s_i^j & 0 \\ s_i^j & c_i^j & 0 \\ 0 & 0 & 0 \end{bmatrix}. \quad (25)$$

Since each  $S_i(t)$  was computed assuming  $q_i(0; k) = 0$ , we include the rotation  $R_i(\tilde{q}_i)$  when constructing  $M_i(t)$  to ensure we only consider trajectories that start from the correct initial condition. For different joint axes,  $M_i(t)$  can be constructed accordingly [6, Chapter 3.2.3].

Importantly,  $M_i(t)$  satisfies the following property:

**Lemma 24.** *For any parameterized trajectory  $q : T \rightarrow Q$  with  $k_i^v = \dot{\tilde{q}}$ , every  $R_i(q_i(t; k)) \in M_i(t)$*

*Proof:* By Lem. 21, all values attained by the sines and cosines of the joint angles are contained in each  $J_i(t)$ . By Alg. 1 and (21), each  $S_i(t)$  only contains the values of sine and cosine of  $q(t; k)$  for which  $k_i^v = \dot{\tilde{q}}$ . Since  $M_i(t)$  only reshapes  $S_i(t)$ , the proof is complete. ■

We use each  $M_i(t)$  with an overapproximation of the forward occupancy map (1) to overapproximate the RS of each link  $\mathcal{L}_i$  with rotatopes  $V_i(t)$ . Given the joint displacements  $l_i$  and link volumes  $L_i$  from Def. 2, we specify  $l_j \in \mathbb{R}^3$  as a zonotope with center  $l_j$  and no generators and  $L_i$  as a zonotope that overapproximates the volume of link  $i$ . Then, we have

**Lemma 25.** *For any  $t \in T$  and  $k \in K$ , the forward occupancy map (1) of link  $i$  with configuration  $q(t; k)$  is overapproximated by the rotatope  $V_i(t)$ :*

$$\text{FO}_i(q(t; k)) \subseteq V_i(t) = \bigoplus_{j < i} \left( \prod_{n \leq j} M_n(t) \{l_j\} \right) \oplus \left( \prod_{n \leq i} M_n(t) L_i \right), \quad (26)$$

*Proof:* First, notice that (26) is defined analogously to (1). We overapproximate  $L_i$ , and have  $R_i(q_i(t; k)) \in M_i(t)$  from Lem. 24. The product of matrix zonotopes multiplied by a zonotope is a rotatope by Lem. 12 and the Minkowski sum of rotatopes are given exactly using Lem. 13. Therefore, all sets and operations in (26) are exact or conservative, so  $\text{FO}_i(q(t; k)) \subseteq V_i(t)$ . ■

As a result of Lem. 25, we can overapproximate the RS of the arm; that is,  $\mathcal{L}_i \subseteq \bigcup_{t \in T} V_i(t) \implies \mathcal{L} \subseteq \bigcup_{i, t} V_i(t)$ .

We compute each  $V_i(t) = (x_i^v(t), \hat{g}_i^j(t), \langle \hat{\beta}_i^j(t) \rangle)^{p(t)}$  using Alg. 2. Many of the generators of  $V_i(t)$  are  $k^a$ -sliceable, because they are products of  $k^a$ -sliceable matrix zonotope generators. Formally, a rotatope generator  $\hat{g}_i^j(t)$  is  $k^a$ -sliceable if there exists at least one  $\langle \kappa_j^a(t) \rangle \in \langle \hat{\beta}_i^j(t) \rangle$  with  $n \leq i$ . This means, by fixing the remaining parameter  $k^a$  via slicing, we obtain a subset of  $V_i(t)$ . We make the distinction that a generator  $\hat{g}_i^j(t)$  is *fully- $k^a$ -sliceable* if all of its indeterminates are evaluated by slicing by  $k^a$ , i.e.  $\langle \hat{\beta}_i^j(t) \rangle \subseteq \bigcup_{n \leq i} \langle \kappa_n^a(t) \rangle$ . Fully- $k^a$ -sliceable generators are created through the multiplication of  $k^a$ -sliceable generators with each other and/or with centers (which have no associated indeterminates) in (26). These generators are important because their indeterminates are evaluated by  $k^a$ , which is the decision variable for our implemented online trajectory optimization.

Notice that the number of generators (and indeterminates) of  $V_i(t)$  increases exponentially with the number of joints, due to the products of matrix zonotopes in (26).

**Remark 26.** *We conservatively approximate (26) by reducing the number of generators after each product, with the `reduce`*

---

**Algorithm 2**  $\{V_i(t) : i = 1, \dots, n_q, t \in T\} = \text{composeRS}(\tilde{q}, \tilde{q})$ 

---

```
1: parfor  $t \in T, i = 1 : n_q$  // parallel for each time step and joint
2:    $\kappa_i^y(t) \leftarrow (\dot{\tilde{q}} - \overline{k}_i^y) / (\Delta k_i^y)$  // get value for (21)
3:    $S_i(t) \leftarrow \text{slice}(J_i(t), \langle \kappa_i^y(t) \rangle)$  // slice JRS
4:    $M_i(t) \leftarrow \text{makeMatZono}(S_i(t), \tilde{q})$  // see (23)
5:    $V_i(t) \leftarrow M_i(t)L_i$  // init  $V_i(t)$  for link volume RS
6:    $U_i(t) \leftarrow l_{i-1}$  // init rotatotope for joint location
7:   for  $j = (i-1) : -1 : 1$  // predecessor joints
8:      $V_i(t) \leftarrow M_j^t V_i(t)$  // rotate link volume
9:      $U_i(t) \leftarrow M_j^t U_i(t)$  // rotate joint location
10:     $V_i(t) \leftarrow \text{reduce}(V_i(t)), U_i(t) \leftarrow \text{reduce}(U_i(t))$ 
11:  end for
12: end parfor
13: parfor  $t \in T$  // parallel for each time step
14:   for  $i = 1 : n_q$  // for each joint
15:     for  $j = (i-1) : -1 : 1$  // predecessor joints
16:        $V_i(t) \leftarrow V_i(t) \oplus U_j(t)$  // "stack" link on joints
17:     end for
18:   end for
19: end parfor
```

---

function in Alg. 2 implemented as in [25, Proposition 2.2 and Heuristic 2.1]. From Lem. 22, each  $M_i(t)$  has  $k$ -sliceable generators. If a  $k$ -sliceable generator is chosen for reduction, we no longer consider it  $k$ -sliceable. This is a conservative approach, because slicing reduces the volume of a rotatotope in Alg. 1. A generator that is no longer  $k$ -sliceable cannot decrease the volume of the RS for any choice of  $k^a$ .

2) *Constraint Generation*: We utilize each rotatotope  $V_i(t)$  to find the set of trajectory parameters that can cause collisions. Specifically, we seek conditions to test whether the subset of  $V_i(t)$  corresponding to a particular  $k^a$  could intersect an obstacle  $O \in \mathcal{O}$  as in Def. 7. For implementation, we assume that each  $O \in \mathcal{O}$  is overapproximated by a zonotope, which is always possible for compact, bounded sets [25]. We formalize these conditions as a collection of constraints to be used in an online optimization program.

Lem. 15 and Rem. 16 provide a useful condition to test if two zonotopes intersect. We explain the condition for intersection of an arbitrary zonotope  $Z = (x, g^j, \langle \beta^j \rangle)^p \subset W$  with an obstacle  $O$ , then show how this extends to sliced rotatotopes. First, we let the generators of  $Z$  define a zero-centered zonotope  $Z_{\text{buf}} = (0, g^j, \langle \beta^j \rangle)^p$ , then buffer the obstacle  $O$  by  $Z_{\text{buf}}$ :  $O_{\text{buf}} = O \oplus Z_{\text{buf}}$ . Note that  $Z = \{x\} \oplus Z_{\text{buf}}$ . Let  $A_{\text{buf}}$  and  $b_{\text{buf}}$  be the half-space representation of  $O_{\text{buf}}$  (Rem. 16). Then,  $Z \cap O \neq \emptyset \iff A_{\text{buf}}x - b_{\text{buf}} \leq 0$ , with the inequality understood element-wise. Conversely,

$$Z \cap O = \emptyset \iff -\max\{A_{\text{buf}}x - b_{\text{buf}}\} < 0. \quad (27)$$

Next, we have that a sliced rotatotope is still a rotatotope, and any rotatotope can be overapproximated by a zonotope by Lem. 14. Therefore, we may use the same test to overapproximate the intersection of any  $V_i(t)$  sliced by  $k^a$  with each  $O \in \mathcal{O}$ . In our implementation, we only slice the fully- $k^a$ -sliceable generators of  $V_i(t)$ . We treat all other generators conservatively as not sliceable, by using them to buffer obstacles. To this end, we

separate  $V_i(t)$  into two rotatotopes:

$$V_{i,\text{slic}}(t) = (x_i(t), g_{\text{slic}}^j, \langle \kappa_{\text{slic}}^j \rangle) \text{ and } V_{i,\text{buf}}(t) = (0, g_{\text{buf}}^n, \langle \beta_{\text{buf}}^n \rangle), \quad (28)$$

such that  $V_i(t) = V_{i,\text{slic}}(t) \oplus V_{i,\text{buf}}(t)$ , where  $V_{i,\text{slic}}(t)$  has only fully- $k$ -sliceable generators. That is, each  $\langle \kappa_{\text{slic}}^j \rangle$  is a product of *only*  $\langle \kappa_i^a(t) \rangle$  for one or more  $i \in \{1, \dots, n_q\}$ .

**Remark 27.** For any  $k^a \in K^a$ , since every generator of  $V_{i,\text{slic}}(t)$  is  $k^a$ -sliceable,  $V_{i,\text{slic}}(t)$  slices to a point. We express this as a function  $\text{eval} : \mathcal{P}(W) \times K^a \rightarrow \mathbb{R}^3$  for which

$$\text{eval}(V_{i,\text{slic}}(t), k^a) = \text{slice}(V_{i,\text{slic}}(t), \{\langle \kappa_i^a(t) \rangle\}_{i=1}^{n_q}, \{\kappa(i)\}_{i=1}^{n_q}) \quad (29)$$

where  $\kappa(i) = (k_i^a - \overline{k}_i^a) / \Delta k_i^a$ . Importantly,  $\text{eval}$  can be implemented as the evaluation of polynomials.

Now let  $A_{\text{obs}}$  and  $b_{\text{obs}}$  be the halfspace representation of  $O_{\text{buf}} = O \oplus V_{i,\text{buf}}(t)$ , and let  $x = \text{eval}(V_{i,\text{slic}}(t), k^a)$ . Then, in analogy to (27), we have:

$$(x \oplus V_{i,\text{buf}}(t)) \cap O = \emptyset \iff -\max\{A_{\text{obs}}x - b_{\text{obs}}\} < 0 \quad (30)$$

where  $x \oplus V_{i,\text{buf}}(t)$  is overapproximated as a zonotope. This statement provides a conservative condition to determine if a given  $k^a$  could cause a collision between  $V_i(t)$  and  $O$ .

We use (30) to overapproximate the set of parameters  $K_{\text{obs}}$  (17) that could cause the arm to collide with any  $O \in \mathcal{O}$  at any time  $t \in T$  using a constraint function  $h_{\text{obs}} : \mathbb{N} \times T \times \mathcal{O} \times K^a \rightarrow \mathbb{R}$ :

$$h_{\text{obs}}(*, k^a) = -\max\{A_{\text{obs}}(*)\text{eval}(V_{i,\text{slic}}(t), k^a) - b_{\text{obs}}(*)\}. \quad (31)$$

where  $* = (i, t, O)$  for space. Here,  $A_{\text{obs}}(i, t, O)$  and  $b_{\text{obs}}(i, t, O)$  return the halfspace representation of  $O \oplus V_{i,\text{buf}}(t)$ . Importantly, for each obstacle, time, and joint,  $h_{\text{obs}}$  is a max of a linear combination of polynomials in  $k^a$  (per Rem. 27), so we can take its subgradient with respect to  $k^a$  [28].

We note that these constraints conservatively approximate the unsafe set:

**Lemma 28.** If  $k^a \in K_{\text{obs}}$ , then there exists  $i \in \mathbb{N}$ ,  $t \in T$ , and  $O \in \mathcal{O}$  such that  $h_{\text{obs}}(i, t, O, k^a) \geq 0$ .

*Proof:* This follows from Lem. 15 and Lem. 25;  $h_{\text{obs}}$  is positive when the zonotope produced by slicing  $V_i(t)$  intersects  $O$ , and  $V_i(t)$  provably contains all points in workspace reachable by the arm under the trajectory parameterized by  $k^a$ . ■

We represent self-intersection constraints similarly, with a function  $h_{\text{self}} : \mathbb{N} \times \mathbb{N} \times T \times K^a \rightarrow \mathbb{R}$ . Suppose  $(i, j) \in I_{\text{self}} \subset \mathbb{N}^2$  indexes a pair of links that could intersect, whose volume is overapproximated by  $V_i(t)$  and  $V_j(t)$ . In analogy to (28), define

$$V_{\text{self}}(i, j, t) = V_{i,\text{slic}}(t) \oplus (-V_{j,\text{slic}}(t)) \text{ and} \quad (32)$$

$$V_{\text{buf}}(i, j, t) = V_{i,\text{buf}}(t) \oplus V_{j,\text{buf}}(t), \quad (33)$$

where  $-V_{j,\text{slic}}(t)$  means the center and generators are multiplied by  $-1$ . Let  $A_{\text{self}}(i, j, t)$  and  $b_{\text{self}}(i, j, t)$  return the half-space representation of  $V_{\text{buf}}(i, j, t)$ . Then, using  $*$  in place of the arguments  $(i, j, t)$  for space,

$$h_{\text{self}}(*, k^a) = -\max(A_{\text{self}}(*)\text{eval}(V_{\text{self}}(*), k^a) - b_{\text{self}}(*)). \quad (34)$$

---

**Algorithm 3**  $q_{\text{plan}} = \text{makePlan}(\tilde{q}, \dot{\tilde{q}}, q_{\text{prev}}, \mathcal{O}, I_{\text{self}}, \varphi)$

---

- 1:  $\{V_i(t)\} \leftarrow \text{composeRS}(\tilde{q}, \dot{\tilde{q}})$  // Sec. IV-B1
  - 2:  $(h_{\text{obs}}, h_{\text{self}}, h_{\text{lim}}) \leftarrow \text{makeCons}(\tilde{q}, \dot{\tilde{q}}, \mathcal{O}, I_{\text{self}}, \{V_i(t)\})$  // Sec. IV-B2
  - 3: // solve (35) within  $t_{\text{plan}}$  or else return  $q_{\text{prev}}$
  - 4:  $q_{\text{plan}} \leftarrow \text{optTraj}(\varphi, h_{\text{obs}}, h_{\text{self}}, h_{\text{lim}}, t_{\text{plan}}, q_{\text{prev}})$  // Sec. IV-B3
- 

As with  $h_{\text{obs}}$ ,  $h_{\text{self}}$  is a max of a linear combination of polynomials in  $k^a$ , so we can take the subgradient with respect to  $k^a$ . Note one can prove a similar result to Lem. 28 for  $h_{\text{self}}$ .

Finally, we construct constraints  $h_{\text{lim}} : K^a \rightarrow \mathbb{R}$  for joint limits. In the trajectory parameterization (11),  $q(t; k)$  is piecewise quadratic in  $k$  and  $\dot{q}(t; k)$  is piecewise linear in  $k$ , so the maxima and minima of the trajectories can be computed by checking the endpoints and local minima of each piecewise function. We construct  $h_{\text{lim}}$  directly, using  $\dot{q}_i$ ,  $q_{i, \text{lim}}$ , and  $\dot{q}_{i, \text{lim}}$ , such that  $h_{\text{lim}}(k^a) < 0$  when feasible.

3) *Trajectory optimization*: We implement (20) as a nonlinear program, denoted  $\text{optTraj}$  in Alg. 3.

$$\begin{aligned}
 & \underset{k^a \in K^a}{\text{argmin}} && f(k^a) \\
 & \text{s.t.} && h_{\text{obs}}(i, t, O, k^a) < 0 \quad \forall i \in \{1, \dots, n_q\}, t \in T, O \in \mathcal{O} \\
 & && h_{\text{self}}(i, j, t, k^a) < 0 \quad \forall (i, j) \in I_{\text{self}}, t \in T \\
 & && h_{\text{lim}}(k^a) < 0 \quad \forall i \in \{1, \dots, n_q\}.
 \end{aligned} \tag{35}$$

**Theorem 29.** *Any feasible solution to (35) parameterizes a trajectory that is collision-free and obeys joint limits over the time horizon  $T$ .*

*Proof:* The conservatism of  $h_{\text{obs}}$  and  $h_{\text{self}}$  follow from Lem. 14 and Remark 16, since each  $J_i(t)$  is conservatively transformed into  $V_i(t)$ . We specify that  $h_{\text{lim}}$  is conservative by construction. ■

### C. Safe Receding-Horizon Planning

ARMTD uses Alg. 3 at each planning iteration. Recall that, without loss of generality, each iteration generates a plan over the time horizon  $T = [0, t_f]$  (by shifting the current time to 0). Each iteration is allotted  $t_{\text{plan}}$  s to run (see Assum. 6). The initial position and velocity of each joint in each iteration is the position and velocity at time  $t_{\text{plan}}$  from the trajectory plan of the previous iteration. ARMTD attempts to find a safe trajectory within  $t_{\text{plan}}$  by optimizing over a set of safe trajectory parameters; Thm. 29 ensures that any feasible solution is actually collision-free. If no safe trajectory is found within the allotted time, the arm executes the braking maneuver specified by the previous safe trajectory. Assuming the arm does not start in collision, this algorithm ensures that the arm is always safe (see [14, Remark 70] or [12, Theorem 1]).

## V. DEMONSTRATIONS

We demonstrate ARMTD in both simulation and hardware using the Fetch mobile manipulator (Fig. 1). A video is available at <https://youtu.be/ySnux2ow1AA>.

To assess the difficulty of our simulated environments, we also ran CHOMP [7] via MoveIt [29] using the default settings

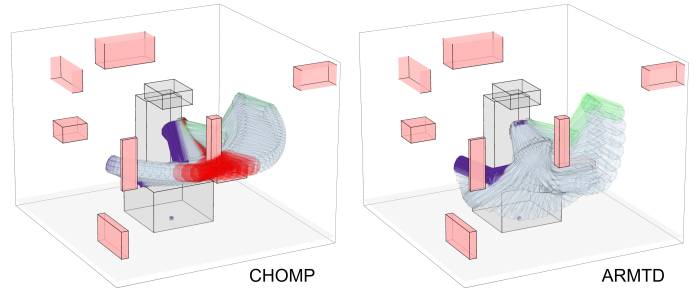


Fig. 3: A Random Obstacles scene with 8 obstacles in which CHOMP [7] converged to a trajectory with a collision (collision configurations shown in red), whereas ARMTD successfully navigated to the goal (green) with a straight-line path planner; the start pose is shown in purple. CHOMP fails to move around a small obstacle close to the front of the Fetch.

and a straight-line initialization. We emphasize that CHOMP in MoveIt is not a receding-horizon planner [29]; it attempts to find a plan from start to goal with a single optimization program. Though the planning paradigms differ, CHOMP provides a useful baseline to measure the performance of ARMTD.

### A. Implementation Details

The Fetch robot arm has 7 DOFs, each described by a revolute joint that is independently actuated (see [1] for detailed specifications). We consider 6 DOFs for ARMTD; the 7th controls end effector orientation, and does not affect the volume used to check collisions. The Fetch arm is composed of 3 physical links, which we model as connected via virtual links of zero volume. Joint limits protect the 1st and 2nd physical links from self-intersection, as well as the 2nd and 3rd; however, we use ARMTD to protect against collision of the 1st physical link with the 3rd. For the hardware demo, we communicate with the Fetch via ROS [30] over WiFi. ARMTD is implemented in MATLAB, CUDA, and C++ running on a 3.6 GHz computer with an Nvidia Quadro RTX 8000 GPU.

1) *JRS Computation*: In practice, the conservatism of each JRS increases with larger values of  $\Delta k_i^v$  and  $\Delta k_i^a$ . This is because (9) is nonlinear with respect to  $k_i^v$  and  $k_i^a$  as in (11), and linearization error is overapproximated when computing the JRS. To minimize conservatism, we set  $K_i^v$  and  $K_i^a$  as follows, given  $\dot{q}_{i, \text{lim}}$  and  $\ddot{q}_{i, \text{lim}}$  as in Assumption 5. Instead of computing a single JRS for  $K_i^v = [-\dot{q}_{i, \text{lim}}, \dot{q}_{i, \text{lim}}]$ , we partition  $K_i^v$  into  $n_{\text{JRS}} \in \mathbb{N}$  equally-sized intervals and compute one JRS for each interval. At runtime (in each planning iteration), we pick which JRS to use for planning based on the current speed of each joint (see Alg. 2 in Sec. IV). Within each JRS, we set

$$\Delta k_i^a = \max \{ r_{a,2}, r_{a,1} \cdot \overline{|k_i^v|} \} \tag{36}$$

with  $r_{a,1}, r_{a,2} > 0$  so that the range of accelerations scales with the absolute value of the mean velocity of each JRS above a certain threshold. This parameterization reduces conservatism of JRSs computed for low speeds, improving maneuverability when close to obstacles. To implement acceleration limits (i.e., to bound  $K_i^a$ ), we specify

$$K_i^a = \left[ \max \{ -\ddot{q}_{i, \text{lim}}, \overline{k_i^a} - \Delta k_i^a \}, \min \{ \ddot{q}_{i, \text{lim}}, \overline{k_i^a} + \Delta k_i^a \} \right], \tag{37}$$

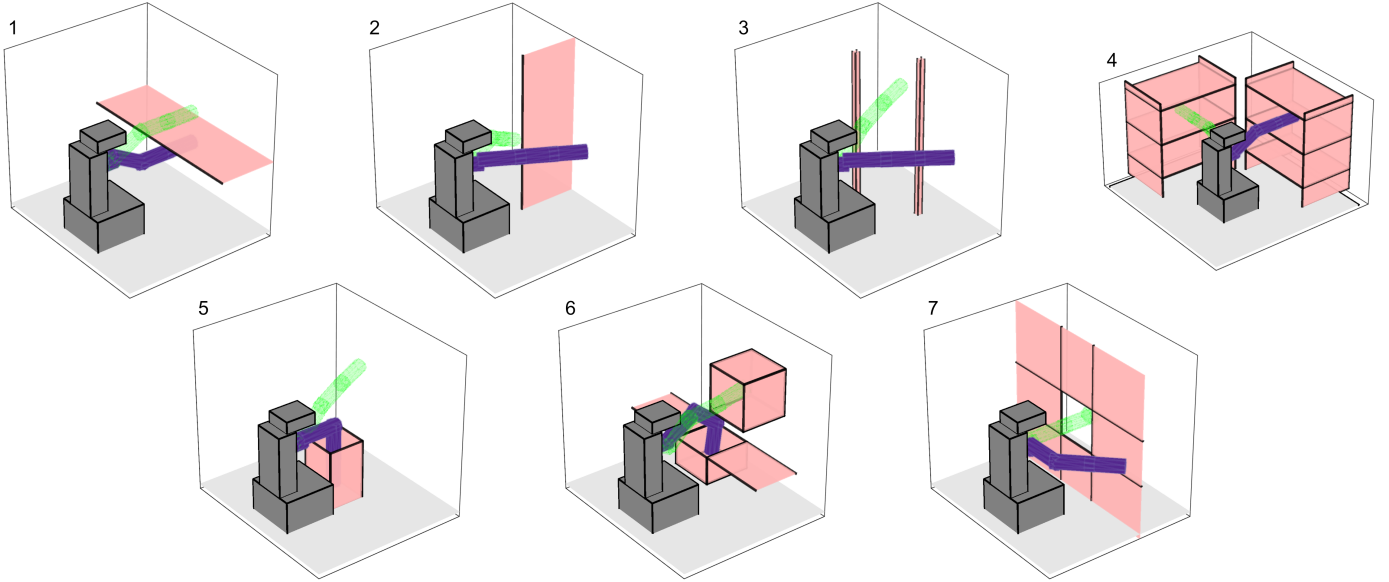


Fig. 4: The set of seven Hard Scenarios (number in the top left), with start pose shown in purple and goal pose shown in green.

for each JRS.

2) *Constraint Generation and Online Optimization*: Alg. 2 is implemented at the start of each ARMTD planning iteration. The operations in each time step in Alg. 2 do not depend on any other time step, making the algorithm well-suited to parallelization. We use a GPU with CUDA to execute Alg. 2 in parallel, which takes approximately 10-20 ms to compose the RS of the entire arm.

Next, we generate constraints using obstacles  $\mathcal{O}$ . Again, this step is parallelizable across obstacles and time steps, and also takes approximately 10-20 ms for 20 obstacles. Self-intersection constraints are also generated in parallel for each time step. Each constraint is computed and stored offline before the online optimization program is solved at each iteration.

We solve the nonlinear program (35) using IPOPT [31]. We specify the cost function  $f$  as minimizing the configuration space distance  $\|q(t_f; k) - q_{\text{des}}\|_2^2$ , where  $q_{\text{des}}$  is a waypoint specified by a path planner at each planning iteration (e.g. an RRT or a straight-line planner, which returns a waypoint along a straight line in configuration space in the direction of a goal configuration relative to a given configuration). We compute analytic gradients/subgradients of the cost/constraints, and evaluate the constraints in parallel as well. Currently, IPOPT takes approximately 100-200 ms when it finds a feasible solution in a scene with 20 random obstacles.

3) *Numerical Details*: We use the following values for our simulation and hardware implementations:  $t_{\text{plan}} = 0.5$  s,  $t_f = 1.0$  s,  $\Delta t = 0.01$  s,  $n_{\text{JRS}} = 400$ ,  $\dot{q}_{i,\text{lim}} = \pi$ ,  $\ddot{q}_{i,\text{lim}} = \pi/3$ ,  $\bar{k}_i^a = 0$ ,  $r_{a,1} = 1/3$ , and  $r_{a,2} = \pi/24$ . Details of the Fetch arm are available [1]. We overapproximate its links, for collision checking, with cylinders of radius 0.146 m.

## B. Simulations

We created two sets of scenes in MATLAB to test ARMTD in simulation. Then, we imported scenes to MoveIt to compare against the CHOMP planner.

1) *Setup*: The first set of scenes, Random Obstacles, shows ARMTD can handle arbitrary tasks. An example scene is shown in Fig 3. This set contains 100 scenes, where a random start and goal configuration are chosen in the Fetch’s configuration space. Box-shaped obstacles, with side lengths varying from 1 to 50 cm, are randomly placed throughout the workspace. Ten scenes are generated with four obstacles, ten with eight obstacles, and so on up to 40 obstacles. The obstacles are not in collision with the Fetch in both the start and goal configurations, nor is the arm in self-intersection (note that MoveIt requires that the goal is not in collision, whereas ARMTD does not).

The second set, Hard Scenarios, shows that ARMTD can guarantee safety where CHOMP converges to an unsafe trajectory. There are seven tasks in the Hard Scenarios set, in which the arm must move: (1) from below to above a table, (2) from one side of a vertical wall to another, (3) between two vertical posts, (4) from one set of shelves to another, (5) from inside to outside of a box on the ground, (6) from a sink to a cupboard, (7) through a small window. These scenarios are shown in Fig. 4.

2) *Results*: We first discuss the Random Obstacles results. Table I compares the performance of ARMTD with a straight-line planner (attempting to follow a straight line between start and goal in configuration space) and an RRT planner against CHOMP with a straight-line initialization. We give results for the mean solve time (MST) of ARMTD per planning iteration, while the MST presented for CHOMP is the time taken to plan a full trajectory. Furthermore, we compare the mean normalized path distance (MNPD) of the trajectories produced by each planner, which is the mean of the cumulative length

of each path divided by the distance between the start and goal in configuration space. For example, a path that follows the straight line from start to goal has a normalized path distance of 1.

In the Random Obstacles scenarios, ARMTD records 84/100 goals and 0/100 crashes with the straight-line planner, while CHOMP records 82/100 goals and 18/100 crashes. We count trajectories where CHOMP converges to a trajectory with a collision as a crash; in practice, the trajectory is collision-checked in MoveIt beforehand and not executed if a collision is detected. Note, it is not always clear what parameters of CHOMP to tune to cause it to converge to a collision-free trajectory without potentially changing its solve time. Because CHOMP and ARMTD follow different planning paradigms, it is difficult to compare them on the basis of their mean solve times; we simply point out that ARMTD’s mean solve times are less than  $t_{\text{plan}} = 0.5$ , meaning that ARMTD usually finds a new plan in each iteration. The MNPD of the plans generated by ARMTD are 24% smaller than those generated by CHOMP. This implies that ARMTD chooses more direct plans from start to goal than CHOMP.

The Hard Scenarios results are as follows (see Table II). Here, ARMTD with a straight-line planner does not complete any of the tasks but also does not crash (the arm gets stuck in a safe configuration from where no new plan can be found). CHOMP converges to trajectories with collisions in all scenarios, hence the name Hard Scenarios. ARMTD, equipped with an RRT\* path planner [32], completes the task in 5/7 scenarios. In each planning iteration, the RRT\* planner generates an end-effector path, then picks a waypoint (in  $W$ ) up to 0.1 m along the path towards the goal. We use MATLAB’s `fmincon` solver for collision-unaware inverse kinematics to find a desired configuration that reaches this waypoint; thus, the RRT\* planner often gives ARMTD waypoints that are in collision. ARMTD tracks the path safely *while the RRT\* is growing*, showing that ARMTD provides real-time safety on top of a potentially unsafe path planner.

### C. Hardware

See the video of ARMTD on the Fetch hardware at <https://youtu.be/ySnux2ow1AA>. ARMTD completes arbitrary tasks while safely navigating the Fetch arm around obstacles (represented for ARMTD in MATLAB), in scenarios are similar to Hard Scenarios (1) and (4). As shown in the simulations, ARMTD was able to render an arbitrary path planner safe, by using an RRT\*, as discussed above, to generate waypoints. ARMTD’s real-time performance was demonstrated by suddenly introducing obstacles in front of the robot arm while it is moving. These obstacles (a box, a vase, and a quadrotor) were tracked using motion capture and treated by ARMTD as static in each planning iteration. Since ARMTD performs receding-horizon planning, it was able to react to each obstacle’s sudden appearance and plan around it without crashing.

Random Obstacles	% goals	% crashes	MST [s]	MNPD
ARMTD	84	0	0.273	1.076
CHOMP	82	18	0.177	1.511

TABLE I: MST is mean solve time (per planning iteration for ARMTD, total for CHOMP) and MNPD is mean normalized path distance. MNPD is only computed for trials where the task was successfully completed, i.e. the path was valid.

Hard Scenarios	1	2	3	4	5	6	7
ARMTD + SL	S	S	S	S	S	S	S
ARMTD + RRT*	O	O	O	S	O	S	O
CHOMP + SL	C	C	C	C	C	C	C

TABLE II: Results for the seven Hard Scenarios simulations (one per column). ARMTD is reported using a straight-line (SL) path planner and an RRT\* path planner. CHOMP is reported using a straight-line initialization. The entries are “O” for task completed, “C” for a crash, or “S” for stopping safely without reaching the goal.

## VI. CONCLUSION

This work proposes ARMTD as a real-time planner with safety guarantees. The method leverages zonotope reachability analysis and parallel computing to generate reachable sets of a robotic arm at runtime, and plans in a receding-horizon way. ARMTD is able to act as a safety layer on top of unsafe path planners, as demonstrated in over a hundred simulations and several hardware demos. Furthermore, ARMTD is able to outperform the existing CHOMP planner in terms of task completion and safety, while not requiring much more planning time. Of course, ARMTD has limitations: it may not perform in real time without parallelization, is only demonstrated on 6-DOF planning problems, and has not yet been demonstrated planning around humans. However, the results in this work show promise for future results in provably-safe robotic arm trajectory planning.

## REFERENCES

- [1] M. Wise, M. Ferguson, D. King, E. Diehr, and D. Dymesich, “Fetch and freight: Standard platforms for service robot applications,” in *Workshop on Autonomous Mobile Service Robots*, 2016.
- [2] F. Pfeiffer and R. Johanni, “A concept for manipulator trajectory planning,” *IEEE Journal on Robotics and Automation*, vol. 3, no. 2, pp. 115–123, Apr. 1987, View online.
- [3] S. Vaskov\*, S. Kousik\*, H. Larson, F. Bu, J. Ward, S. Worral, M. Johnson-Roberson, and R. Vasudevan, “Time-Optimal Trajectory Generation for Path Following with Bounded Acceleration and Velocity,” in *Robotics: Science and Systems*, 2018.
- [4] S. M. LaValle and J. J. Kuffner Jr., “Randomized kinodynamic planning,” *The International Journal of Robotics Research*, vol. 20, no. 5, pp. 378–400, 2001.
- [5] L. E. Kavraki, P. Svestka, J.-C. Latombe, and M. H. Overmars, “Probabilistic roadmaps for path planning in high-dimensional configuration spaces,” *IEEE transactions on Robotics and Automation*, vol. 12, no. 4, pp. 566–580, 1996.
- [6] S. M. LaValle, *Planning Algorithms*. New York, NY, USA: Cambridge University Press, 2006.
- [7] M. Zucker, N. Ratliff, A. D. Dragan, M. Pivtoraiko, M. Klingensmith, C. M. Dellin, J. A. Bagnell, and S. S. Srinivasa, “Chomp: Covariant hamiltonian optimization for motion planning,” *The International Journal of Robotics Research*, vol. 32, no. 9-10, pp. 1164–1193, 2013.

- [8] J. Schulman, Y. Duan, J. Ho, A. Lee, I. Awwal, H. Bradlow, J. Pan, S. Patil, K. Goldberg, and P. Abbeel, "Motion planning with sequential convex optimization and convex collision checking," *The International Journal of Robotics Research*, vol. 33, no. 9, pp. 1251–1270, 2014.
- [9] C. Park, J. Pan, and D. Manocha, "Itomp: Incremental trajectory optimization for real-time replanning in dynamic environments," 2012, View online.
- [10] S. Murray, W. Floyd-Jones, Y. Qi, D. J. Sorin, and G. Konidaris, "Robot Motion Planning on a Chip," in *Robotics: Science and Systems*, 2016.
- [11] T. Kunz, U. Reiser, M. Stilman, and A. Verl, "Real-time path planning for a robot arm in changing environments," in *2010 IEEE/RSJ International Conference on Intelligent Robots and Systems*, Oct. 2010, pp. 5906–5911.
- [12] K. Hauser, "On responsiveness, safety, and completeness in real-time motion planning," *Autonomous Robots*, vol. 32, no. 1, pp. 35–48, Jan. 2012.
- [13] A. Majumdar and R. Tedrake, "Funnel libraries for real-time robust feedback motion planning," *ArXiv preprint arXiv:1601.04037*, 2016.
- [14] S. Kousik, S. Vaskov, F. Bu, M. Johnson-Roberson, and R. Vasudevan, "Bridging the Gap Between Safety and Real-Time Performance in Receding-Horizon Trajectory Design for Mobile Robots," *ArXiv e-prints arXiv:1809.06746*, Sep. 2018.
- [15] S. Kousik, P. Holmes, and R. Vasudevan, "Safe, Aggressive Quadrotor Flight via Reachability-Based Trajectory Design," *Dynamic Systems and Control Conference*, vol. 3, Oct. 2019, V003T19A010.
- [16] M. Althoff, A. Giusti, S. B. Liu, and A. Pereira, "Effortless creation of safe robots from modules through self-programming and self-verification," *Science Robotics*, vol. 4, no. 31, 2019.
- [17] T. G.A. A. A. Singletary P. Nilsson, "Online Active Safety for Robotic Manipulators," in *2019 IEEE/RSJ International Conference on Intelligent Robots and Systems (IROS)*, Nov. 2019.
- [18] S. L. Herbert, M. Chen, S. Han, S. Bansal, J. F. Fisac, and C. J. Tomlin, "FaSTrack: A modular framework for fast and guaranteed safe motion planning," in *2017 IEEE 56th Annual Conference on Decision and Control (CDC)*, Dec. 2017, pp. 1517–1522.
- [19] M. Chen, S. L. Herbert, M. S. Vashishtha, S. Bansal, and C. J. Tomlin, "Decomposition of Reachable Sets and Tubes for a Class of Nonlinear Systems," *IEEE Transactions on Automatic Control*, vol. 63, no. 11, pp. 3675–3688, Nov. 2018.
- [20] D. Meagher, "Geometric modeling using octree encoding," *Computer graphics and image processing*, vol. 19, no. 2, pp. 129–147, 1982.
- [21] J.-M. Lien and N. M. Amato, "Approximate convex decomposition of polyhedra," in *Proceedings of the 2007 ACM symposium on Solid and physical modeling*, 2007, pp. 121–131.
- [22] T. Kunz and M. Stilman, "Towards Provably Not-at-Fault Control of Autonomous Robots in Arbitrary Dynamic Environments," in *Robotics: Science and Systems*, 2012.
- [23] M. Althoff, "An Introduction to CORA 2015," in *Proc. of the Workshop on Applied Verification for Continuous and Hybrid Systems*, 2015.
- [24] L. J. Guibas, A. Nguyen, and L. Zhang, "Zonotopes as bounding volumes," in *Proceedings of the fourteenth annual ACM-SIAM symposium on Discrete algorithms*, Society for Industrial and Applied Mathematics, 2003, pp. 803–812.
- [25] M. Althoff, "Reachability analysis and its application to the safety assessment of autonomous cars," PhD thesis, Technische Universität München, 2010.
- [26] B. Paden and R. Panja, "Globally asymptotically stable PD+controller for robot manipulators," *International Journal of Control*, vol. 47, no. 6, pp. 1697–1712, 1988.
- [27] A. Giusti and M. Althoff, "Efficient Computation of Interval-Arithmetic-Based Robust Controllers for Rigid Robots," in *2017 First IEEE International Conference on Robotic Computing (IRC)*, Apr. 2017, pp. 129–135.
- [28] S. Boyd, L. Xiao, and A. Mutapcic, "Subgradient methods," *Lecture notes of EE392o, Stanford University, Autumn Quarter*, vol. 2004, pp. 2004–2005, 2003.
- [29] D. Coleman, I. A. Sucas, S. Chitta, and N. Correll, "Reducing the Barrier to Entry of Complex Robotic Software: a MoveIt! Case Study," *CoRR*, vol. abs/1404.3785, 2014.
- [30] M. Quigley, K. Conley, B. Gerkey, J. Faust, T. Foote, J. Leibs, R. Wheeler, and A. Y. Ng, "ROS: an open-source Robot Operating System," in *ICRA workshop on open source software*, Kobe, Japan, vol. 3, 2009, p. 5.
- [31] A. Wächter and L. T. Biegler, "On the implementation of an interior-point filter line-search algorithm for large-scale nonlinear programming," *Mathematical programming*, vol. 106, no. 1, pp. 25–57, 2006.
- [32] S. Karaman and E. Frazzoli, "Sampling-based algorithms for optimal motion planning," *The international journal of robotics research*, vol. 30, no. 7, pp. 846–894, 2011.